Int J Adv Manuf Technol (2009) 42:126–137
DOI 10.1007/s00170-008-1587-1

ORIGINAL ARTICLE

Visual sensing and penetration control in aluminum alloy pulsed GTA welding

Chongjian Fan · Fenglin Lv · Shanben Chen

Received: 28 January 2008 / Accepted: 27 May 2008 / Published online: 16 July 2008

Abstract In this paper, visual sensing and penetration control in aluminum (Al) alloy pulse gas tungsten arc welding were researched. Firstly, a three-optical-route visual sensor was designed. The sensor can capture the weld pool from three directions at the same time. After analyzing the influences of different factors on weld pool image, serials of clear and stable weld pool images were obtained. Then, image processing technologies were developed to compute back topside weld pool geometry parameters. Wavelet transform and Canny operator were synthesized to get all edges in the weld pool image. After noise removal and calibration, the breaking edges of weld pool were obtained, and then piecewise curve fitting based on polynomial function were used to recover the whole weld pool edge. Lastly, proportional–integral–differential and a multiplex controller were designed to control penetration in welding process. Experiments proved that visual-based penetration control can insure welding quality well from weld pool width and reinforcement.

Keywords Visual sensing · Penetration control · Image processing · Welding

1 Introduction

Aluminum (Al) alloy gas tungsten arc welding (GTAW) plays an important role in the industrial production. However, aluminum alloys are very sensitive to heat input and heat conducting. It is difficult to ensure good penetration in aluminum alloy automatic welding. So researches in automatic welding are necessary in application.

Sensing technology is an important part in automatic welding. But it is well known that welding is difficult to inspect in real time. Different information were researched in penetration control, such as ultrasonic, aural signal, arc voltage, and so on [1–4]. Chin B. A. did a lot of work in spot infrared thermograph sensor. The sensor can measure the temperature field of the arc, bead, molten pool, and its variation. His study has been used in penetration control of GTAW and submerged arc [5–7]. But welding process is very complex. High temperature, extensive arc light, and noise in welding process will make most sensing methods invalid.

Visual sensing is one of the most prosperous ways in penetration sensing now [8]. Most information can be captured into charge coupled device (CCD) camera through this method. The information is nearly as abundant as welder's eyes. The only problem remains in how to filter off the strong arc light. There are two ways to solve the problem. One is to use projected laser. Kovacevic and Zhang did penetration control in GTAW by observing weld pool with laser projection [8–11]. In fact, most lasers are line scanning in application. It is more fitting for seam tracking than penetration control.

The other way is to develop optical filter technology. It is to use CCD to "see" weld pool directly as the welder. In this way, useless light can be filtered and useful light remains to light the weld pool. This has been researched widely in seam tracking and penetration control in different welding methods. Kim et al. [12] designed a long wave pass filter so that arc intensity was reduced and weld pool width was observed for penetration control in GTAW. Ohshima measured the weld pool geometry by visual

C. Fan (✉) · F. Lv · S. Chen
Institute of Welding Engineering, Shanghai JiaoTong University,
No. 800, Dongchuan Rd., Minhang,
Shanghai 200240, People's Republic of China
e-mail: chj_fan@sjtu.edu.cn

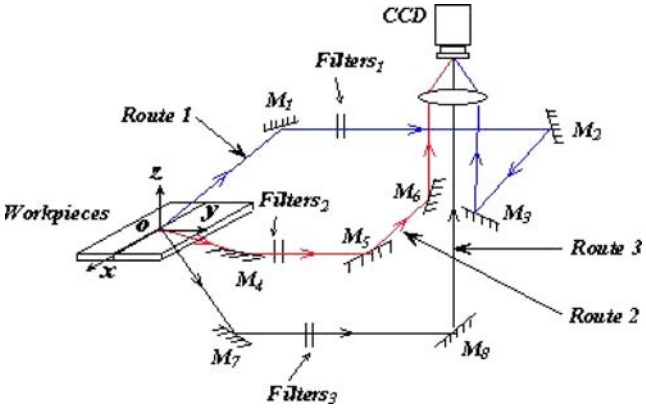

Fig. 1 The three light routes of simultaneous visual sensing system of weld pool in a frame

sensor during base current in gas metal arc welding (GMAW) [13]. Kuo and Wu [14] used fuzzy logic and optical technology to attempt tracking welding seam. But it was done before welding. Bae et al. [15] designed an optical system for seam tracking and weld pool control in GMAW. In fact, their research is mainly on seam tracking. The sensor cannot obtain clear weld pool. Zhao et al. [16] attempted to calculate molten weld pool surface height and other parameters to describe the penetration during pulse GTAW. S. B. Chen et al. [17] systematically introduced the whole welding control system in pulse GTAW from optical sensor, model to controller design.

All the works above are on the mild steel welding [8–17]. It is more difficult for optical sensing in aluminum alloy welding. There are at least two reasons. One is that aluminum alloy is more sensitive for heat conduction but its melting point is lower. Welding parameters adjustment should react more quickly. And aluminum alloy color does not change much during its molten process. Wang attempted to get the images for the first time, but most molten pool information could not be seen from his images due to strong arc light [18].

In this study, the main work includes two parts: optical sensing and penetration control in welding process. "Section 2" introduces the weld pool visual sensing. A special three-light-route optical sensor was introduced. It can get weld pool image from three directions in one frame. Some factors were analyzed to insure better quality of the weld pool. "Section 3" introduces how to get information from images. A new algorithm-synthesizing wavelet transform (WT) and Canny operator is developed in "Section 3.1." After noise removal and calibration, piecewise curve fitting based on polynomial function were used to recover the whole weld pool edges. In "Section 4," different controllers were designed in welding process under different conditions. Their advantages and shortcomings were analyzed carefully.

2 Optical sensor and weld pool image

To study the relation between weld pool geometry shape and penetration, a three-route optical visual sensor was developed. The sensor can capture the weld pool from two sides (three directions) of the workpiece: topside (including front topside and back topside) and backside in one frame in real time. Through route 1 (back topside), the whole weld pool can be observed. Through route 2 (front topside),

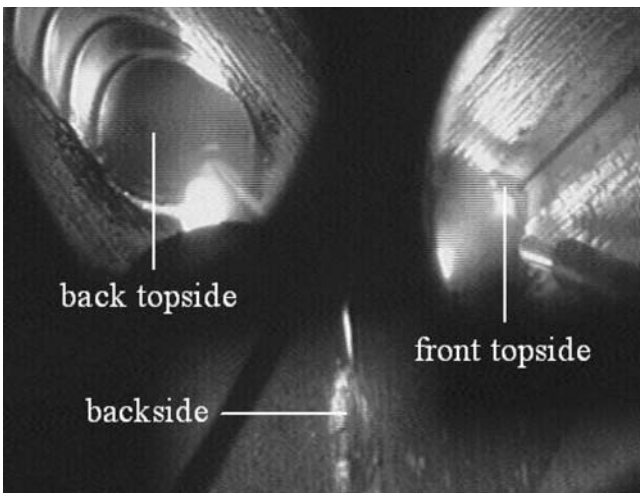

Fig. 2 The three-direction image

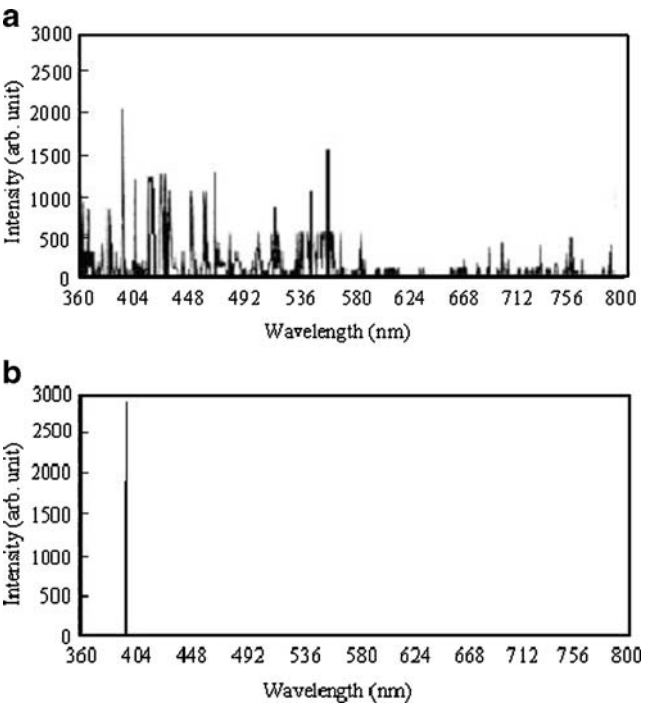

Fig. 3 Standard spectrum of Ar and Al

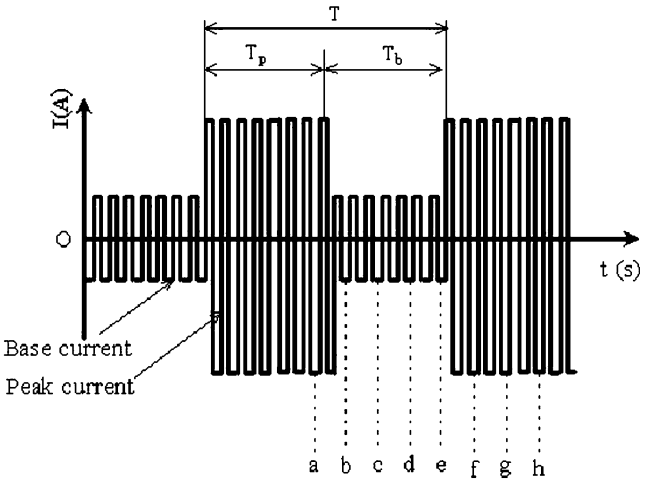

Fig. 4 The oscillograph of the welding current

workpiece gap and welding direction can be observed. Through route 3 (backside), the back of weld pool and penetration can be observed. The definitions of the three routes and images were pointed out in Fig. 1. *Mi*(*i*= 1,2,⋯,8) is reflecting mirror. After the second (backside) or third (front topside and back topside) reflection, lights entered CCD separately at the same time through the three routes from weld pool. The weld pool image is shown in Fig. 2. The weld pool is observed from three directions at the same time by one CCD.

In welding process, intensive arc light makes it difficult for us to observe the weld pool. So there must be some preconditions for the visual sensing.

1. Filter system: filter system consists of ultrared filter glass and neural density filter. Standard spectrums of argon (Ar) and Al are shown in Fig. 3, separately.

When wavelength is shorter than 580 nm, Ar spectrum is very complicated and there are many strong discontinuous spectral lines in different wavelength. If only those strong Ar spectral lines are used as lighting resource, experiments proved that the weld pool image is unstable whether the

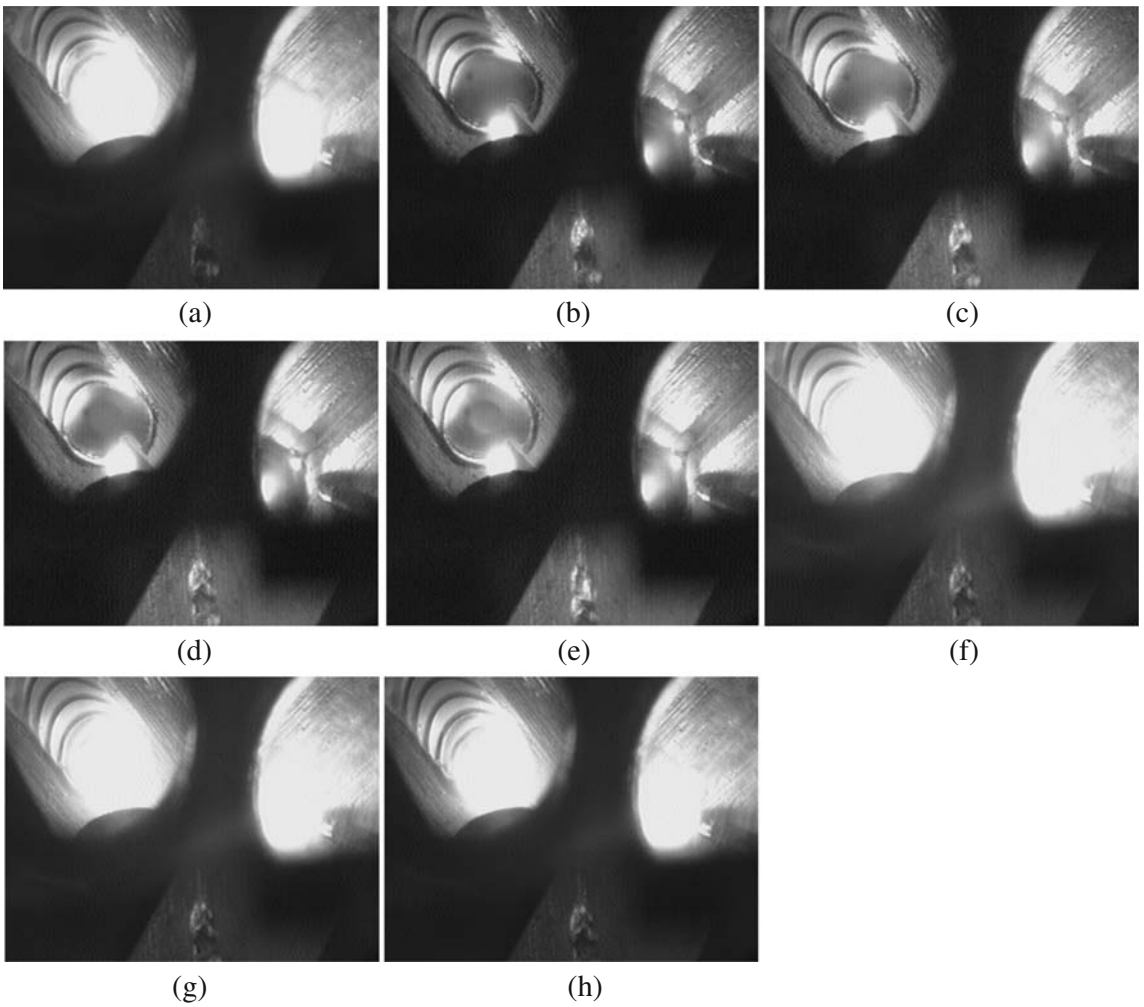

Fig. 5 The consecutive images in a period

filtering window is wide or narrow because their discontinuous intensities are always changing. If wavelength is longer than 600 nm, the spectrum continuity is better so the light resource is more stable. If filtering window is too wide, the image contrast is low and weld pool is not distinctive. More experiments proved that, if narrow band pass window of the filter system is from 710 to 730 nm, weld pool can be observed clearly and stably. Moreover, the neutral density filter permits only 10% arc light reflecting into CCD. Both ultrared filter glass and neutral density filter glass assured weld pool image clearly and stably from light source.

2. The time of obtaining image: From technology, alternating current (AC) is necessary for aluminum alloy GTAW because AC can remove oxide film on aluminum surface in welding process. Pulse is necessary for observing weld pool. Under pulse AC, when current is at peak level, arc light is still very intensive even though there is filter system. When current is at base level, weld pool can be observed well.

Figure 4 is the oscillograph of the pulse AC which was used in the experiments. The pulse period are T=0.5 s and T_p=T_b 0.25 s. In one pulse period, eight images were taken during welding. Each time the images were taken, a, b,···, h were drawn in Fig. 4, and images at each time were given in Fig. 5. The interval between adjacent time points is 60 ms. Time b is 50 ms from after the peak current changing to base current. In welding process, both current and welding wire affects the weld pool. The weld pool is not stable when the time is earlier than b but still in base current because high current and wire at the earlier peak affect the surface of weld pool. As time goes on after b, the light becomes more and more intensive and it makes the images less and less clear. This also proves that the current becomes higher from time b to e. But the variation is relatively small. So time b is selected as observing time due to its clear images.

3. Base current: base welding current affects weld pool image seriously. High current causes weld pool images to be too bright while low current causes weld pool image to be too dark. Furthermore, arc is not stable if current is lower than 40 A. Different images under corresponding base currents are given in Fig. 6. These images and corresponding experiments proved that the weld pool image is acceptable when base current range is 40~60 A. So 50 A is selected as base current.

In Fig. 7, series of consecutive images were given to observe penetration from incomplete to excessive in a GTAW process. Welding and capturing image parameters are: peak current 235 A and base current 50 A; the time, when observing weld pool, is 50 ms after peak current turned to base current. The period of welding current is 0.5 s. For aluminum alloy butt welding with wire feeding, weld pool length is short when penetration is incomplete. When penetration becomes more complete, weld pool length becomes longer. At the same time, weld pool width and back width becomes wider, too.

Figure 2 is a complete frame image containing three-direction images. Weld pool and other details around it are

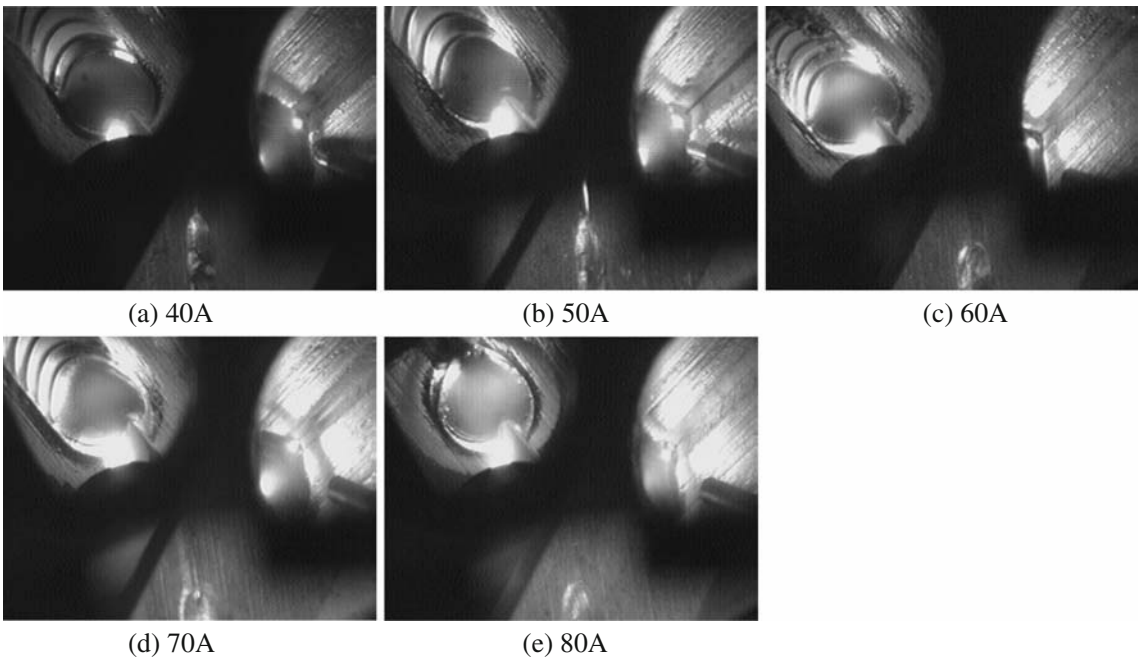

Fig. 6 Images under different base current

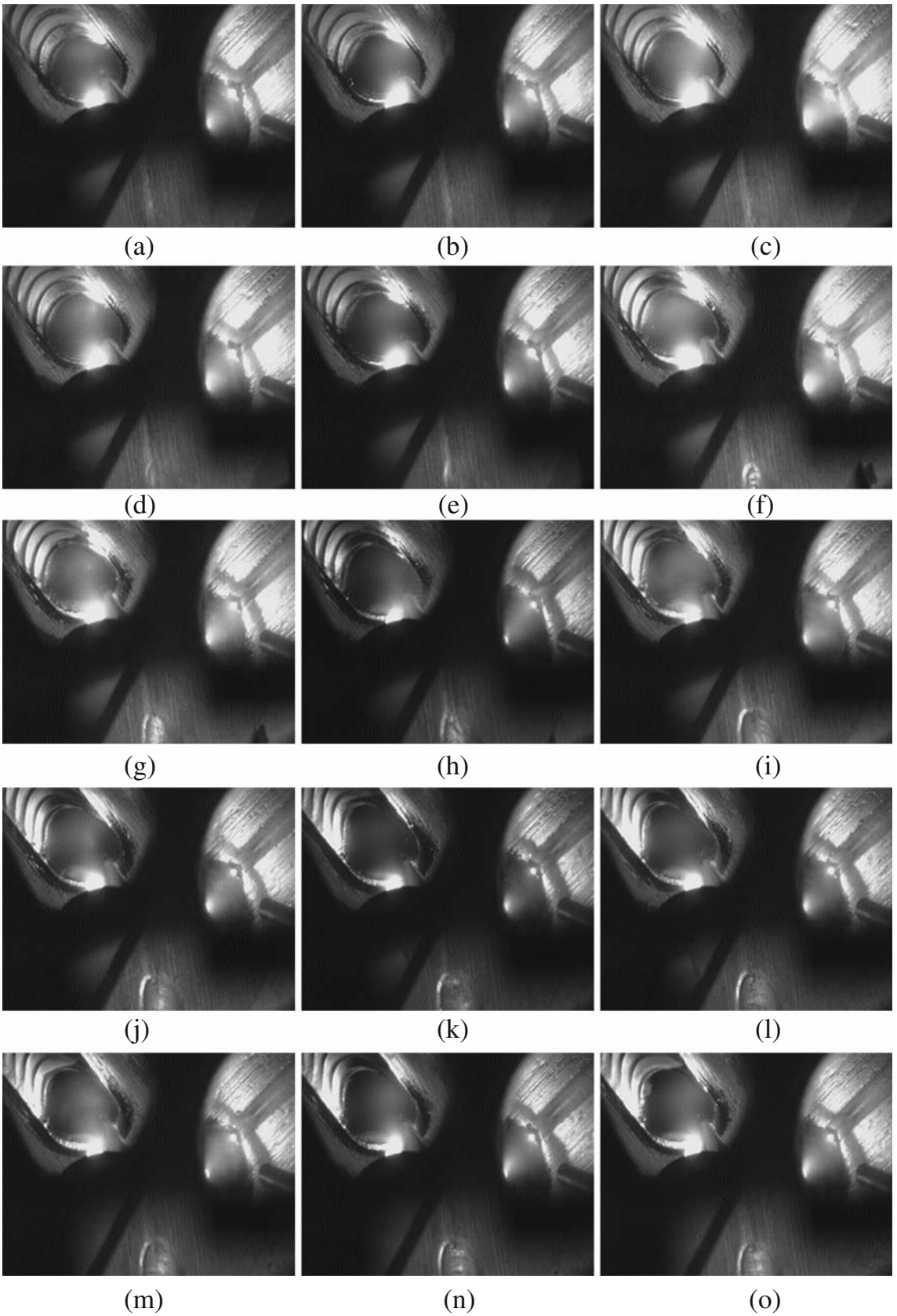

Fig. 7 Images from incomplete weld pool to excessive

all clear. The back topside weld pool image contains most pool information, but it is also the most difficult to process. In this study, back topside weld pool images will be processed first.

3 Image processing

Since wavelet transform (WT) has advantages such as antinoise and precise edge localization, it is good for edge detection [19]. In this paper, we presented a scale-multiplication-based edge detection scheme. Moreover, Canny operator is also an excellent algorithm because its edge detection result is precise and continuous and has a width of single point. In this study, we try to combine the advantages of these two techniques together in weld pool image processing.

3.1 Scale-multiplication-based edge detection

Directly multiplying the dyadic wavelet transform (DWT) at adjacent scales will dilute the noise. But if three or more adjacent scales were incorporated in the multiplication, edges would not be sharpened more but much edge dislocation would occur. So it is appropriate to analyze the multiplication using two scales [19–21].

Suppose $\theta(x, y)$ is a two-dimensional differentiable smooth function whose integral is 1 and converges to 0 at infinity. A function $\psi(x, y)$ is called a wavelet if its average is equal to 0 [22, 23].

The DWT of $f(x, y)$ at dyadic scale 2^j and position (x, y) is $\psi^1(x, y)$ and $\psi^2(x, y)$. The two wavelets are:

$$\psi^1(x,y) = \frac{\partial\theta(x,y)}{\partial x}, \psi^2(x,y) = \frac{\partial\theta(x,y)}{\partial y} \tag{1}$$

where $\theta(x,y) = e^{\frac{x^2+y^2}{2\delta^2}}, \delta = 0.5$.

Denote $\zeta_j(x,y) = 2^{-j}\zeta(2^{-j}x, 2^{-j}y)$, the dilation of $\zeta(x, y)$ by 2^j. The WT of $f(x, y)$ at scale 2^j and position (x, y) has two components

$$W_j^1 f(x,y) = f * \psi_j^1(x,y), W_j^2 f(x,y) = f * \psi_j^2(x,y) \tag{2}$$

where * denotes convolution operation and ζ_j denotes the dyadic dilation of function ζ. The scale product functions of $f(x, y)$ are defined as the correlation of two adjacent DWT scales. Two product functions should be defined in x and y directions.

$$\begin{aligned} P_j^{f,1}(x,y) &= W_j^1 f(x,y) W_{j+1}^1 f(x,y), P_j^{f,2}(x,y) \\ &= W_j^2 f(x,y) W_{j+1}^2 f(x,y) \end{aligned} \tag{3}$$

Subscript j means that the correlation is computed as scales 2^j and 2^{j+1}.

For an edge point (x_0, y_0), $W_j^i f(x_0, y_0)$ and $W_{j+1}^i f(x_0, y_0)$, $i = 1, 2$ should have the same sign. So both $P_j^{f,1}(x_0, y_0)$ and $P_j^{f,2}(x_0, y_0)$ will be nonnegative and the orientation information of the gradient is lost, which should be recovered from $W_j^1 f(x_0, y_0)$ and $W_j^2 f(x_0, y_0)$.

Setting the points with $P_j^{f,1}(x,y) < 0 \left(P_j^{f,2}(x,y) < 0\right)$ to 0, the magnitude and orientation of point (x, y) are defined as

$$M_j f(x,y) = \sqrt{P_j^{f,1}(x,y) + P_j^{f,2}(x,y)}, \tag{4}$$

$$A_j f(x,y) = \arctan\left(\frac{\operatorname{sgn}\left(W_j^2 f(x,y)\right) \cdot \sqrt{P_j^{f,2}(x,y)}}{\operatorname{sgn}\left(W_j^1 f(x,y)\right) \cdot \sqrt{P_j^{f,1}(x,y)}}\right) \tag{5}$$

As in the Canny edge detector algorithm, an edge point is asserted wherever $M_j f(x, y)$ has a local maximum in the direction of the gradient given by $A_j f(x, y)$.

In processing the magnitude image array $M_j f(x, y)$, nonmaxima suppression and the double-thresholding algorithm in Canny edge detector are regarded as the best methods. To identify edges, the broad ridges in the magnitude array must be thinned so that only the magnitudes at the points of greatest local change remain. Then the double-thresholding algorithm takes the nonmaxima-suppressed image and applies two thresholds τ_1 and τ_2, with τ_2=0.4τ_1, to produce two thresholded edge images $T_1[x, y]$ and $T_2[x, y]$. Since image T_2 was formed with a higher threshold, it will contain fewer false edges; but T_2 may have gaps in the edge contours (too many false negatives). The double-thresholding algorithm links the edges in T_2 into contours. When it reaches the end of a contour, the algorithm looks in T_1 at the locations of the eight neighbors for edges that can be linked to the contour. The algorithm continues to gather edges from T_1 until the gap has been bridged to an edge in T_2. The algorithm performs edge linking as a byproduct of thresholding and resolves some of the problems with choosing a threshold. In fact, Canny operator mainly includes nonmaxima suppression and the double-thresholding algorithm. The processed edge is continuous and 1-pixel width. For detail of Canny edge detection algorithm, please refer to [24]. Figure 8 is the edge detection result.

3.2 Noise removal

There are some characteristics from the noises in Fig. 8: (1) little noises exists inside of weld pool; (2) noises near pool head and arc are nearly fixed; (3) all other noises exist outside of weld pool, especially on solidified bead.

The corresponding reasons for those noise characteristics are: (1) when taking weld pool image, welding current is at

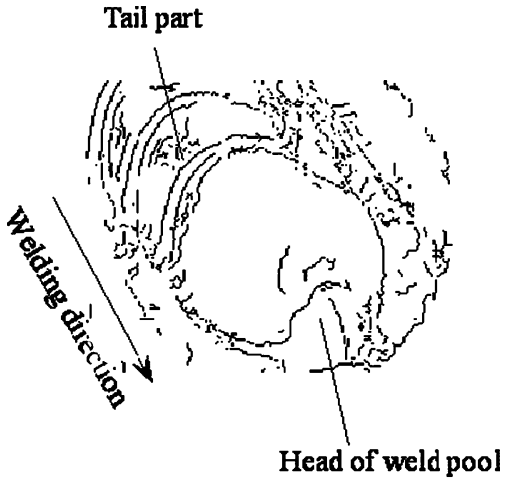

Fig. 8 Edge detection including WD transform and Canny operator

base level, there is no fluctuation on molten weld pool surface. It means that little noises exist inside of the pool; (2) there are some fixed objects such as nozzle, wire feeding, etc. near the pool head and arc. These objects make fixed noises near pool head in the image. (3) On the tail of weld pool, there are solidified pool waves along bead. Most noises in the image are caused by those waves. Other noises are caused by the machined surface of workpiece.

After analyzing those noise characters, we choose the following corresponding methods to remove them:

1. For the noises inside of the weld pool, no removing action was taken. Curve fitting discussed in "Section 3.4" can eliminate their influence;
2. For the noises near pool head, the positions are nearly fixed, so they can be deleted directly by experience;
3. For the noises outside of weld pool, we can remove them by searching method from inside of weld pool to outside. The detailed method is done according to the following steps.

General image coordinate system *XOY* is defined in Fig. 9. Point *o* is the tungsten electrode projecting point on workpiece. *o* is (x_o, y_o) in the image coordinate system. $f(x, y)$ is the gray value of point (x, y). *w* is the width of the image, and *h* is the height. Here, x_o=105, y_o=35.

The first searching method is to search the straight line $y=y_o$ along the two direction of axis *Y* outward.

1. In image coordinate system, use point $(x_o + i, y_o + j)$, $i = -45, j = 0$, as starting point and search along the direction parallel to the positive direction of axis *Y*;
2. j ++, if $j>h$, then turn to 4; if $f(x, y)$=255 and $j\leq h$, then set its $f(x, y)$=1, turn to 3, or turn to 2;
3. if $f(x_o + i + m, y + j + n) = 255, (m, n = 1, 0, 1)$, *set* $f(x + i + m, y + j + n) = 1$;
4. if $i < 45$, i++, turn to 1 or turn to 5;

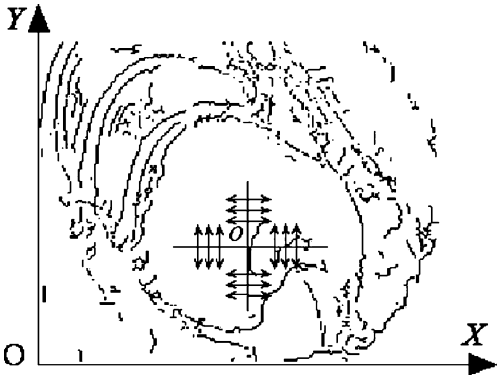

Fig. 9 Searching methods from inside to outside

5. In image coordinate system, use point $(x_o + i, y_o + j)$, $i=-45$, $j=0$, as starting point, search along the direction parallel to the negative direction of axis *Y*;
6. $j-\,-$, if $j<0$, then turn to (8); if $f(x, y)$=255 and $j\geq 0$, then set its $f(x, y)$=1, turn to 7 or turn to 6;
7. if $f(x_o+i+m, y+j+n)$=255 (m, n=−1,0,1), set $f(x+i+m, y+j+n)$=1;
8. if $i<45$, i++, turn to 5 or stop the scanning;

The second searching method searches the two sides of the straight line $x=x_o$ along the two directions of axis *X*. The searching method is similar to the above steps.

After searching twice, if $f(x, y)$=1, then $f(x, y)$=255, and (x, y) is the edge point or $f(x, y)$=0. The searching result is shown in Fig. 10.

3.3 Calibration

In workpiece coordinate system, weld pool is nearly asymmetrical to the center line of the welding seam. But from Fig. 2, weld pool shape and direction in image plane have changed from those on workpiece. Figure 11 is the image after rotating from Fig. 10, and the rotating angle is

Fig. 10 Searching result after special methods based on experience

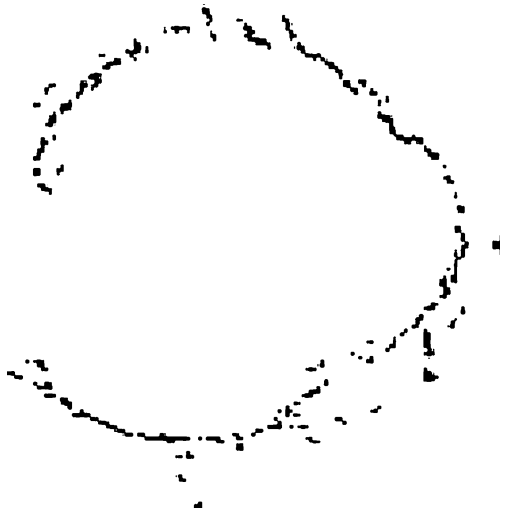

Fig. 11 The deformed image after directly rotating

115°. Obviously, the edge curve is not asymmetrical in this image. So calibration must be applied to recover its edge curve from image plane coordinates to absolute coordinates.

Coordinate system *xoy* on workpiece was defined first in Fig. 12(a). Point *o* is the tungsten electrode projecting point on workpiece. Its positive direction of $\overrightarrow{x}$ is the same as the welding direction; $\overrightarrow{y}$ is vertical to $\overrightarrow{x}$. In image coordinate system, in the direction parallel to $\overrightarrow{y}$, one pixel length means α_y *mm* in absolute workpiece coordinate system. In the direction parallel to $\overrightarrow{x}$, one pixel length means α_x *mm*.

From theory, α_x and α_y is different for every point in the image, respectively. But from calibration experiments, we found that the variations of α_x and α_y are no more than 1% for the points around weld pool, respectively. So α_x and α_y may be regarded as two constants around weld pool.

A new coordinate system $x'o'y'$ is defined in Fig. 12(b); it is the same as *xoy* except for two differences: (1) $\overrightarrow{x'}$ is opposite direction to $\overrightarrow{x}$; $\overrightarrow{y'}$ is opposite direction to $\overrightarrow{y}$. (2) In image plane, $\overrightarrow{x'}$ is vertical to $\overrightarrow{y'}$ while $\overrightarrow{x}$ is not vertical to $\overrightarrow{y}$.

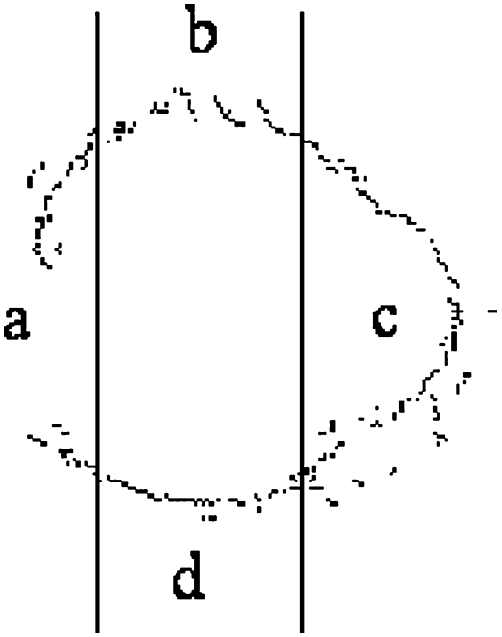

Fig. 13 Piecewise curve fitting

For point A, the transformation from image to $x'o'y'$ is

$$\begin{pmatrix} x_0' \\ y_0' \end{pmatrix} = \begin{pmatrix} -1 & 0 \\ 0 & -\alpha \end{pmatrix} \begin{pmatrix} x_0 \\ y_0 \end{pmatrix} \tag{6}$$

where $\alpha = \frac{\alpha_y}{\alpha_x}$. In Fig. 12(a), point o' is (105, 70). The slope of x is k_x=−1.919; the slope of y is k_y=0.319, α=1.102. Figure 12(b) is the calibrated image.

3.4 Piecewise curve fitting

After calibration, the size of weld pool in the image is α_x times of its real size in workpiece coordinate system. If the pool edge in Fig. 13 can be fitted, its real edge curve of workpiece coordinate can be fitted, too.

For weld pool edge fitting, many studies have discussed it [25–27]. But the methods did not fit for aluminum alloy welding. Since welding process is complicated, no function can fit the whole weld pool edge well.

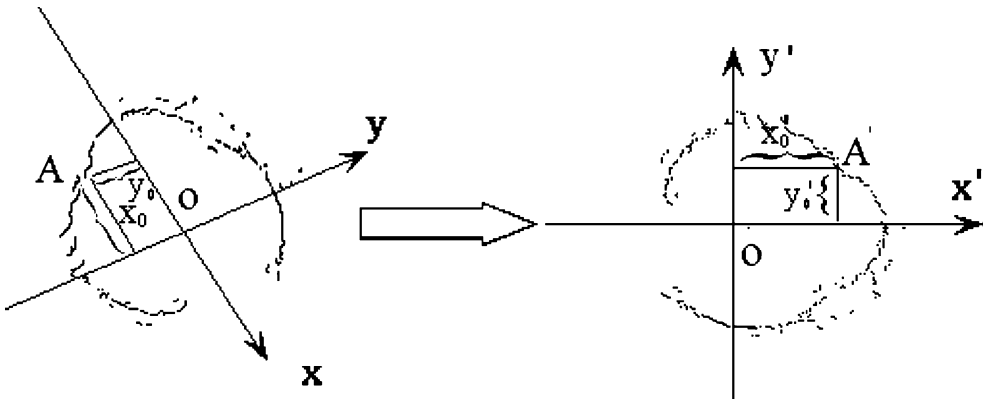

Fig. 12 *a–d* The calibrating process for real weld pool edge recovering

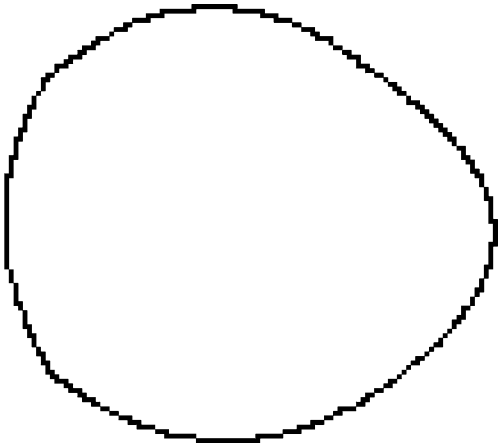

Fig. 14 The fitting result after piecewise curve fitting method

From Fig. 13, the whole weld pool was divided into four parts by two straight lines. Special characteristics were found: edge in every part is similar to a quadratic curve. So polynomial functions,

$$y = a_0x^n + a_1x^{n-1} + \cdots + a_n \text{ or } x = b_0y^n + b_1y^{n-1} + \cdots + b_n, \quad (7)$$

were used to fit every part in this study. Then the weld pool edge can be fitted by connecting the four fitting curves. These functions are linear and the least square method can be used to find their solutions, here, n=2. The solution of the four parts is $(a_0\ a_1\ a_2)$ or $(b_0\ b_1\ b_2)$.

For part a: $(b_0\ b_1\ b_2) = (-0.0075556\ 1.5496\ 17.3791)$,
part b: $(a_0\ a_1\ a_2) = (-0.011287\ 2.4976\ -22.84)$,
part c: $(b_0\ b_1\ b_2) = (0.017114\ -3.512\ 161.6154)$,
part d: $(a_0\ a_1\ a_2) = (0.0095725\ -2.17756\ 128)$.

The curve fitting result is shown in Fig. 14. Lastly, two parameters were defined in Fig. 15: W_f and L_f. W_f is the maximum width of the weld pool. L_f is the maximum distance from tail part of weld pool to the straight line where the weld pool width is the maximum. From Fig. 15, the two parameters can be calculated.

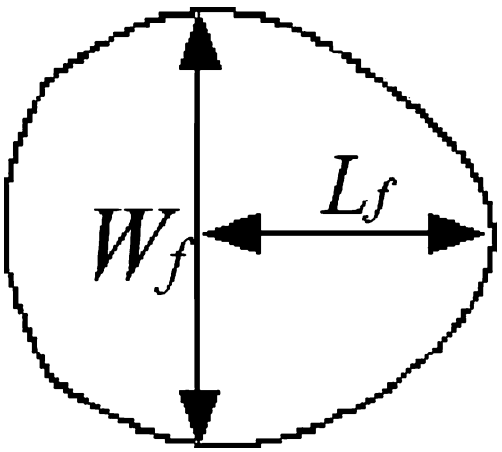

Fig. 15 Weld pool parameters definition

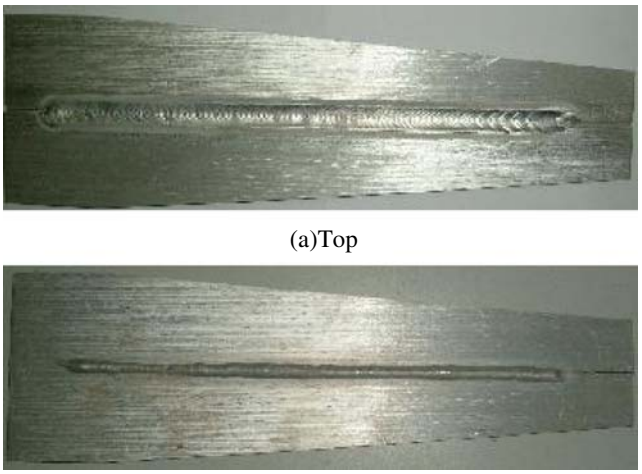

(a)Top

(b)Back

Fig. 16 **a**–**b** Welded workpiece controlled by current PID

4 Experiments and analyses

The welding process control system in this set of experiments consists of a personal computer with data acquisition and control expansion cards installed to interface with the optical sensor, welding power supply, and motion control system. Function such as seam tracking, penetration control, etc. can be carried out.

In application, the back width of weld pool and reinforcement are the best factors in describing penetration while they are too difficult to measure in welding process. In control experiments, the weld pool width is used to control welding process. From experience, when weld pool

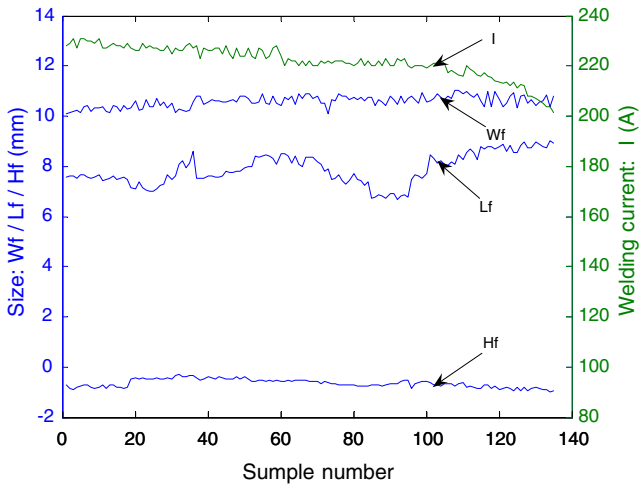

Fig. 17 Variables in welding process

(a)Top

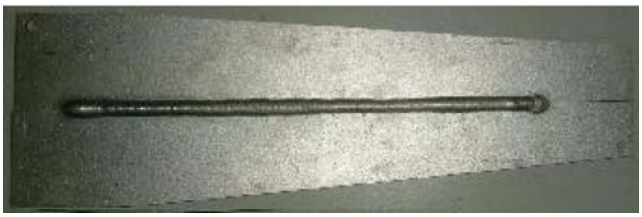

(b)Back

Fig. 18 **a**–**b** Welded workpiece controlled by wire feed rate PID

width is about 10.5 mm, the back width of the weld pool is about 6–7 mm. It means that the penetration is acceptable. So, in experiments, penetration is controlled through controlling weld pool width.

In welding controller design, process model is always the bottleneck. The reason is that welding process is too complicated to be comprehended well. To avoid this problem, proportional–integral–differential (PID) controller was introduced into our study. Many researches have proved that PID can be used in welding quality control and seam tracking [28, 29].

System input is peak current I or wire feed rate V_f while output is weld pool width W_f. Reinforcement H_f, gap width g, and weld pool length L_f are also provided in some figures below. Among these parameters, W_f, L_f, and g are computed from images. For the algorithm of g, please refer to [30]. H_f is measured by micrometer after welding process. Only W_f

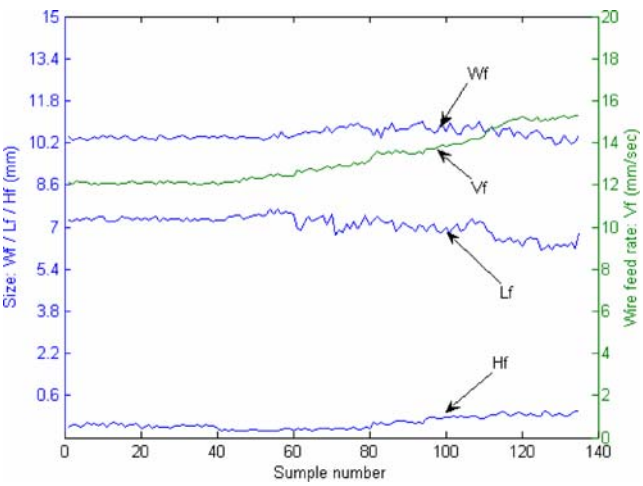

Fig. 19 Variables in welding process

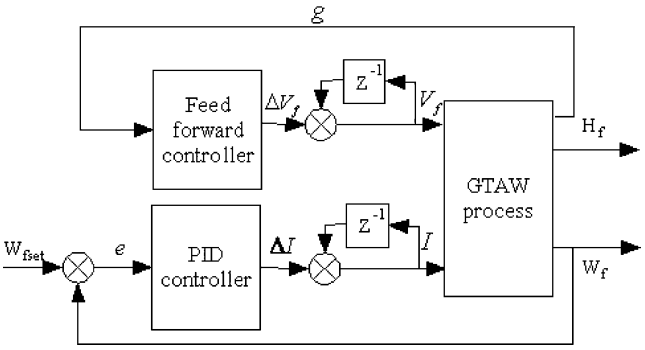

Fig. 20 Multiplex controller with PID and feed forward

and g are used in control, and L_f, H_f are provided to study the welding process control.

From Figs. 16a,b and 17, W_f can be controlled well if welding current is the system input. But H_f is always lower than 0 and the back width of weld pool is a little great. From Figs. 18(a)(b) and 19, if wire feed rate is the system input, W_f can be controlled well. But H_f is better than that in Fig. 17. The welding process reacts more quickly for wire feed rate. L_f changes more quickly than W_f, too. If back width becomes smaller or H_f become greater, L_f becomes smaller. This means that L_f may be regarded as an important parameter in penetration control.

Comparing with the workpiece without control, when controller input is I, penetration is well while sometimes excessive. When controller input is V_f, reinforcement can be assured well while penetration is very acute to V_f.

In fact, if gap width g>0.5 mm, PID controllers above are hardly available because gap width now affects penetration too much. Feed forward controller based on gap feedback should be used here.

There is a difference between this experiment and the two before. A welding backing is used here but not in the two experiments before. If g>0.5 mm, it is difficult to ensure penetration in automatic welding without welding backing. Figure 20 is the multiplex controller with PID and feed forward control. Current I is used to control W_f and V_f is used to control g, separately.

In feed forward controller, V_f is decided by the volume of molten metal. The groove style is shown in Fig. 21. The

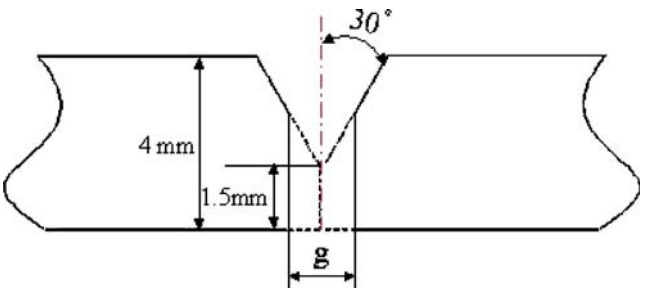

Fig. 21 Groove shape

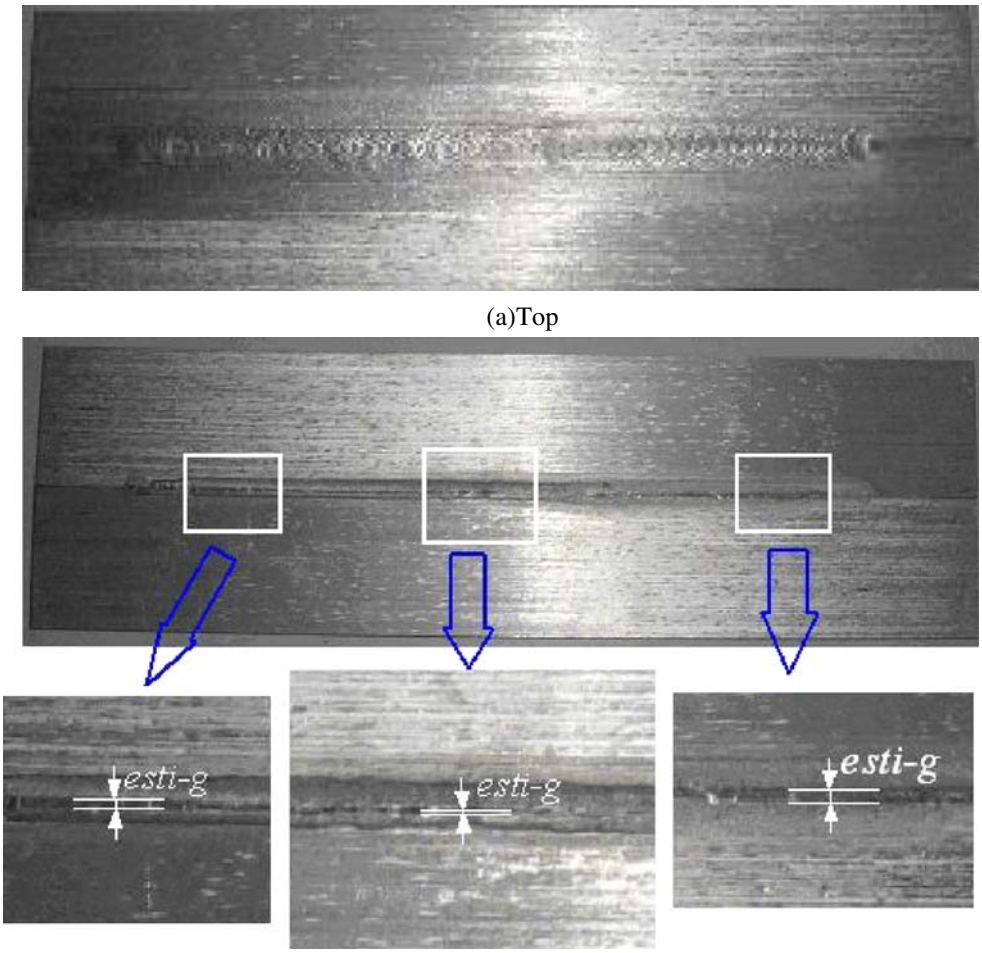

(a)Top

(b)Back

Fig. 22 **a**–**b** Welded workpiece controlled by multiplex controller

ideal gap width is 1.5 mm but actual gap width is g. The feed forward controller can be described as:

$$\Delta V_f = \frac{13.2g}{\pi} \tag{8}$$

From Fig. 22, after welding, the back of weld pool is different if g is different. Different *esti–g* in Fig. 22b meant different g. If there is no gap, *esti–g* equals nearly zero. Penetration is well controlled by the controller even though the gap exists. Especially, H_f is the best among the three experiments. W_f is also the greatest because there are more metal molten in the groove. All variations are shown in Figs. 23 and 24.

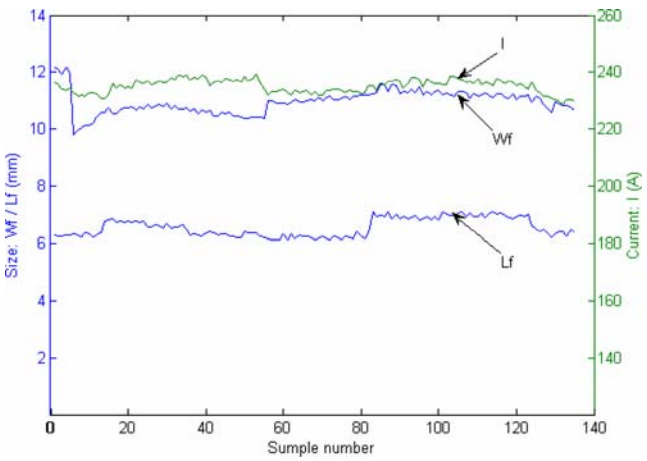

Fig. 23 Variables I in welding process

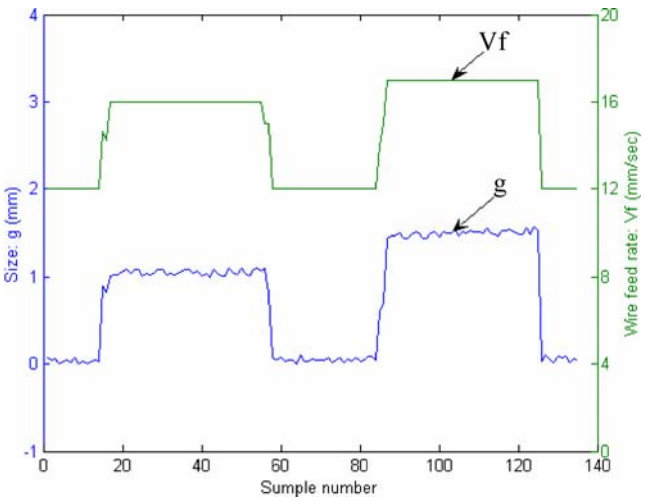

Fig. 24 Variables II in welding process

In the three experiments, the last one is the most stable especially if there is a gap. If there is no gap, the controller equals to the current PID controller. In the first two PID controllers, current PID controller can ensure penetration better while the reinforcement is not so well. Wire feed rate PID controller can ensure reinforcement while penetration is very sensitive to it.

5 Conclusions

In this paper, visual sensing and penetration control in aluminum alloy welding were researched. A three-optical-route visual sensor was designed to capture the weld pool from three directions at the same time. Nearly all details in and around the pool can be distinguished from the images. Then image processing technologies were developed to compute back topside weld pool geometry parameters. Wavelet transform and Canny operator were combined to get all edges in the weld pool image. Then, after noise removal, calibration and piecewise curve fitting are used to recover the whole weld pool edges. Lastly, different controllers were designed to control penetration in welding process. Experiments proved that, when gap is small, PID controller can ensure welding quality whether the input is welding current or wire feed rate and, when gap is big, multiplex controllers were used to ensure weld pool width and reinforcement.

Acknowledgements This work is supported by Chinese National Natural Science Foundation under Grand No. 50575144. It is also supported by Key Foundation Program of Shanghai Sciences and Technology Committee under Grand No. 06JC14036.

References

1. Graham GM Ume CI (1997) Automated system for laser ultrasonic sensing of weld penetration. Mechatronics 7(8):711–721
2. Futamata M (1983) Application of arc sound for detection of welding process. Quarterly Journal of the Japan Welding Society 1(1):11–14
3. Chin BA, Madsen NH, Goodling JS (1983) Infrared thermography for sensing the arc welding process. Weld J 62(9):227–234
4. Chen W, Chin BA (1990) Monitoring joint penetration using infrared sensing techniques. Weld J 69(4):181–185
5. Wikle HC, Kottilingam S, Zee RH, Chin BA (2001) Infrared sensing techniques for penetration depth control of the submerged arc welding process. J Mater Process Technol 113(1–3):228–233 doi:10.1016/S0924-0136(01)00587-8
6. Guu AC, Rokhlin SI (1992) Technique for simultaneous real-time measurements of weld pool surface geometry and arc force. Weld J 71(12):473–482
7. Rokhlin SI, Guu AC (1990) Computerized radiographic sensing and control of an arc welding process. Weld J 69(3):83–95
8. Zhang YM, Kovacevic R, Li L (1996) Characterization and real-time measurement of geometrical appearance of the weld pool. Int J Mech Manuf 36(7):799–816 doi:10.1016/0890-6955(95)00083-6
9. Song HS, Zhang YM (2008) Measurement and analysis of three-dimensional specular gas tungsten arc weld pool surface. Weld J 87(4):85–95
10. Song HS, Zhang YM (2007) Image processing for measurement of three-dimensional GTA weld pool surface. Weld J 86(10):323–330
11. Saeed G, Zhang YM, Jaynes C (2005) Weld pool surface monitoring and depth extraction using a calibrated CCD sensor. ASM Proceedings of the International Conference: Trends in Welding Research 2005:665–670
12. Kim DC, Rhee SH, Um KW (1996) A study of weld pool width control in gas tungsten arc welding using the digital image processing. J. KSMEA 20(9):2760–2769
13. Ohshima K, Yamamoto M, Tanshi T, Yamane S (1992) Digital control of torch position and weld pool in MIG welding using image processing device. IEEE Trans Ind Appl 28(3):607–612 doi:10.1109/28.137446
14. Kuo HC, Wu LJ (2002) An image tracking system for welded seams using fuzzy logic. J Mater Process Technol 120(1–3):169–185 doi:10.1016/S0924-0136(01)01155-4
15. Bae KY, Lee TH, Ahn KC (2002) An optical sensing system for seam tracking and weld pool control in gas metal arc welding of steel pipe. J Mater Process Technol 120(1–3):458–465 doi:10.1016/S0924-0136(01)01216-X
16. Zhao DB, Lou YJ, Chen SB, Wu L (1999) Surface height and geometry parameters for describing shape of weld pool during pulsed GTAW. In: SPIE Proceedings of the 1999 Intelligent System in Design and Manufacturing II, Boston, Massachusetts, USA, vol. V3833, pp 91–98
17. Chen SB, Lou YJ, Wu L, Zhao DB (2000) Intelligent methodology for sensing, modeling and control of pulse GTAW: part 1-bead-on-plate welding. Weld J 79(6):151–163
18. Wang JJ, Lin T, Chen SB (2005) Obtaining weld pool vision information during aluminum alloy TIG welding. Int J Adv Manuf Technol 26(3):219–227 doi:10.1007/s00170-003-1548-7
19. Lei Z, Paul B (2002) Edge detection by scale multiplication in wavelet domain. Patten Recognition letters 23:1771–1784
20. Xu Y et al (1994) Wavelet transform domain filters: a spatially selective noise filtration technique. IEEE Trans Image Process 3:747–758 doi:10.1109/83.336245
21. Sadler BM, Swami A (1999) Analysis of multiscale products for step detection and estimation. IEEE Trans Inf Theory 45:1043–1051 doi:10.1109/18.761341
22. Daubechies I (1992) Ten lectures on wavelets. SIAM, Philadelphia
23. Mallat S, Zhong S (1992) Characterization of signals from multiscale edges. IEEE Trans. PAMI 14:710–732
24. Ramesh J, Rangachar K, Schunck BG (2003) Machine vision. McGraw Hill Education Press and China Machine Press, Beijing
25. Brzakovic D, Khani DT, Awad B (1992) A vision system for monitoring weld pool. In: Proceeding of the 1992 IEEE International Conference on robotics and automation, Nice, France, pp 1609–1614
26. Zhang YM, Li L, Kovacevic R (1997) Dynamic estimation of full penetration using geometry of adjacent weld pools. ASME J Manuf Sci Eng 119(11):631–643 doi:10.1115/1.2831197
27. Zhang GJ (2002) Intelligent control of weld shape during varied gap pulsed GTAW with wire filler based on visual sensing. Doctoral dissertation, Harbin Institute of Technology, China
28. Schmitt DJ, Novak JL, Starr GP et al (1994) Real-time seam tracking for rocket thrust chamber manufacturing. Proceedings-IEEE International Conference on Robotics and Automation 3:2261–2266
29. Huang YW, Tung PC, Wu CY (2007) Tuning PID control of an automatic arc welding system using a SMAW process. Int J Adv Manuf Technol 34(1–2):56–61 doi:10.1007/s00170-006-0569-4
30. Fan CJ, Lv FL, Chen SB (2007) A visual sensing system for welding control and seam tracking in aluminum alloy gas tungsten arc welding. In: IECON 2007—the 33rdAnnual Conference of the IEEE, Taiwan, China, pp. 2700–2705